Femtomolar isothermal desorption using microhotplate sensors

Amol G. Shirke
Department of Chemical and Biological Engineering, University of Maine, Orono, Maine 04469-5737

Richard E. Cavicchi and Steve Semancik
Chemical Science and Technology Laboratory, National Institute of Standards and Technology, Gaithersburg, Maryland 20899-8362

Robert H. Jackson
Stillwater Scientific Instruments, 20 GodFrey Drive, Orono, Maine 04473

Brian G. Frederick
Department of Chemistry, University of Maine, Orono, Maine 04469
and Laboratory for Surface Science and Technology, University of Maine, Orono, Maine 04469

M. Clayton Wheeler[a)]
Department of Chemical and Biological Engineering, University of Maine, Orono, Maine 04469-5737

(Received 10 August 2006; accepted 6 March 2007; published 5 April 2007)

The authors describe a technique that utilizes the fast heating rates (10^6 K/s) of a microhotplate sensor along with a calibrated thermal desorption system to determine the initial coverage and kinetic parameters using isothermal desorption on a millisecond time scale. Models for isothermal desorption including both pumping and desorption rate effects are presented for zero, first, and second order kinetics. Analysis of the first order model illustrates the domain of the desorption, pumping speed, and heating rate time constants that permit the desorption parameters to be estimated from the mass spectrometer signal. The technique is demonstrated using isothermal temperature programed desorption of benzoic acid from a single SnO_2 covered microhotplate at surface temperatures ranging from 296 to 347 K. The data indicate that desorption is best represented by first order kinetics. The first order preexponential factor and the desorption energy in the zero coverage limit are determined to be 1×10^{17} s^{-1} and 97 kJ/mol, respectively, from desorption of 10^8 molecules which corresponds to an initial coverage of 10^{12} cm^{-2} ($\leqslant$0.005 ML).
 [DOI: 10.1116/1.2720850]

I. INTRODUCTION

Techniques for micromachining silicon have led to rapid growth in the area of microelectromechanical systems, many of which are designed to perform sensing and actuating functions.[1] In the 1990s, researchers at the National Institute of Standards and Technology used integrated circuit fabrication technology to fabricate complementary metal-oxide semiconductor compatible microhotplates. A microhotplate is a micromachined structure that can serve as both a gas sensor as well as a surface science research tool.[2] It is a suspended multilayered structure fabricated on a silicon wafer and consists of an integrated heater, a thermal distribution plate, and surface electrodes. Each of these features is separated by an electrical insulating layer. A photomicrograph of a microhotplate is shown in Fig. 1, and schematics of the various fabrication layers and array configurations have been presented elsewhere.[3]

When used as the platform for a gas microsensor, a metal-oxide semiconducting film is typically deposited on top of the surface electrodes of the microhotplate to serve as the active gas-sensing component. The small thermal mass of the hotplate allows heating and cooling rates as high as 10^6 K/s for repetitive temperature changes on the millisecond time scale. This capability has been effectively applied in temperature programed sensing (TPS), a technique in which temperature modulation of the sensing film leads to characteristic conductometric signatures for a particular gas analyte.[2] Meier *et al.*[4] and Boger *et al.*[5] have employed this technique using arrays of microhotplates for sensing warfare agents such as tabun and sarin. The nature of specific TPS signatures are determined by the surface coverage of individual species which in turn are governed by adsorption, desorption, and reaction rates. Therefore, a detailed knowledge of the reaction mechanisms and their effect on sensor electrical properties would aid in designing more selective sensors.

Microhotplates provide an excellent means for relating fundamental surface phenomena to sensing performance. The microhotplate has previously been demonstrated as a platform to study surface reactions and desorption kinetics with metallic thin films, and the millisecond heating times are intermediate to those accessible by traditional temperature programed desorption and pulsed laser desorption techniques.[6] Cavicchi *et al.* developed a pulsed-desorption technique to study desorption kinetics of CO on Pt, which enabled the evaluation of the desorption activation energy and the rate constant simultaneously without the interference

[a)]Author to whom correspondence should be addressed; electronic mail: cwheeler@umche.maine.edu

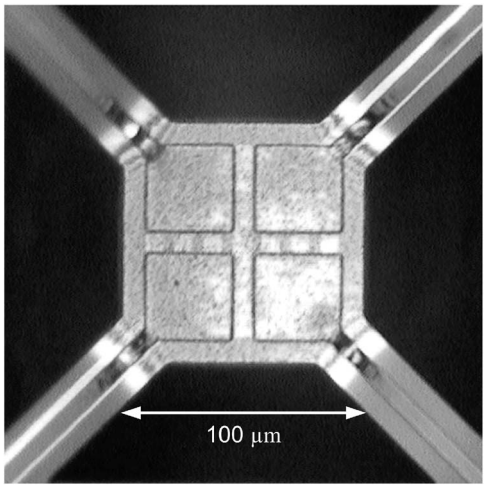

FIG. 1. Photomicrograph of a microhotplate coated with a SnO_2 sensing material.

of the system pumping effects in an ultrahigh vacuum system.[7] The approach required that a relatively large surface area and coverage of the analyte be employed so the desorption could be measured over a series of isothermal pulses. High surface area was accomplished by simultaneously controlling the temperatures of hundreds of microhotplate elements in an array with a cumulative surface area of about 10^{-2} cm^2. The saturation coverage of CO on Pt is approximately 10^{15} cm^{-2}.[8,9]

Measurement of the fundamental desorption kinetic parameters for adsorbates on well-defined single crystal surfaces have been made using thermal desorption, or temperature programed desorption (TPD), since the early work of Redhead[10] (and others cited therein). Several reviews[11–13] discuss the basic formalism, as well as a number of experimental techniques (including linear and nonlinear temperature ramps), and analysis methods (such as the simple leading edge analysis[14] and "complete methods"[15,16]) that extract coverage dependent activation energies and preexponential factors, which can arise due to factors such as lateral interactions.[17] More recently, dynamic Monte Carlo simulations[18–20] are being used to gain greater insight into the complexities of the desorption process, even for relatively well-defined systems.

In 1992, DeAngelis and Anton developed an isothermal TPD method and measured CO desorption on Ni(110).[21] The technique involved adsorbing gas on a clean surface at low temperature, rapidly increasing and maintaining the surface temperature at a higher value where desorption occurs while monitoring the evolution of gas with a mass spectrometer. This technique offered the benefit of mathematical ease for analyzing the desorption curve, since, at constant adsorbent temperature, the time dependent rate is a function of coverage only. In the isothermal TPD approach, ideally little or no desorption should occur during the heating transient. Therefore, the largest desorption rate that can be measured by this "step-TPD" approach is limited by the speed at which the desorption temperature is reached, and DeAngelis and Anton developed a feed-forward/feedback control system to heat their nickel single crystal with a response on the order of a few seconds.

The current work develops and demonstrates a method to estimate the rate constant for desorption from a microsensor (a single microhotplate element) using isothermal TPD. The fast heating rates of the microhotplates and high sensitivity of the differentially pumped mass spectrometer[22] were combined to allow detection of the extremely low coverages expected for adsorption on semiconducting metal-oxide surfaces. Weisz[23] developed a model in 1953 using metal-semiconductor junction analogs that is frequently accepted as the reason that the coverage of certain types of chemisorbed species can be limited on semiconductors. The Weisz model predicts that chemisorption coverage accompanied by charge transfer is limited to about 10^{12} cm^{-2} on a semiconductor. The surface area of a single microhotplate is only 10^{-4} cm^2, although we note that the actual surface area of the granular sensor material on the microhotplate may be larger. Our analysis shows that measurement of kinetic parameters from the isothermal desorption of as little as 10^8 molecules is possible, which is orders of magnitude lower than would be possible with a typical UHV thermal desorption system with a typical metal single crystal of area 1 cm^2 and coverage of 10^{15} cm^{-2}, where a detection limit of 10^{-3} MLs corresponds to 10^{12} molecules. The effects of system pumping had to be considered in the current work because for the highest desorption rates, the pumping and desorption time constants are on the same order of magnitude. In addition, a predictive temperature control method was devised to reduce the heating time constant to 0.2 ms, which was negligible compared to the desorption time constant over a sufficiently large range of isothermal desorption temperatures for quantitative analysis to be performed.

In the current study, isothermal TPD was used to measure benzoic acid desorption rates from a single microhotplate covered by a SnO_2 film as the sensing material. Benzoic acid (C_6H_5COOH) is composed of a benzene ring with a single carboxylic acid group. It was chosen because it is a solid with a low vapor pressure at room temperature that one of us has worked with extensively before[24,25] and was expected to yield a relatively high surface coverage even under ultrahigh vacuum conditions. Indeed, Lee *et al.*, observed multilayer adsorption of benzoic acid on Cu(110) at a surface temperature of 270 K.[26] However, there is no evidence for multilayer adsorption (zero order desorption) in the current study. The isothermal TPD results, which take into consideration the system pumping constraints under conditions in which the heating rate constant can be neglected, show that desorption was first order. The preexponential and activation energy determined are 1×10^{17} s^{-1} and 97 kJ/mol, respectively.

The article is structured as follows. First, we present the experimental setup for isothermal TPD from a microhotplate. Then we develop a model that includes pumping, desorption, and heating rate effects. For first order desorption, we analyze the range of parameter space that allows kinetic information to be determined. Finally, we compare the data to first

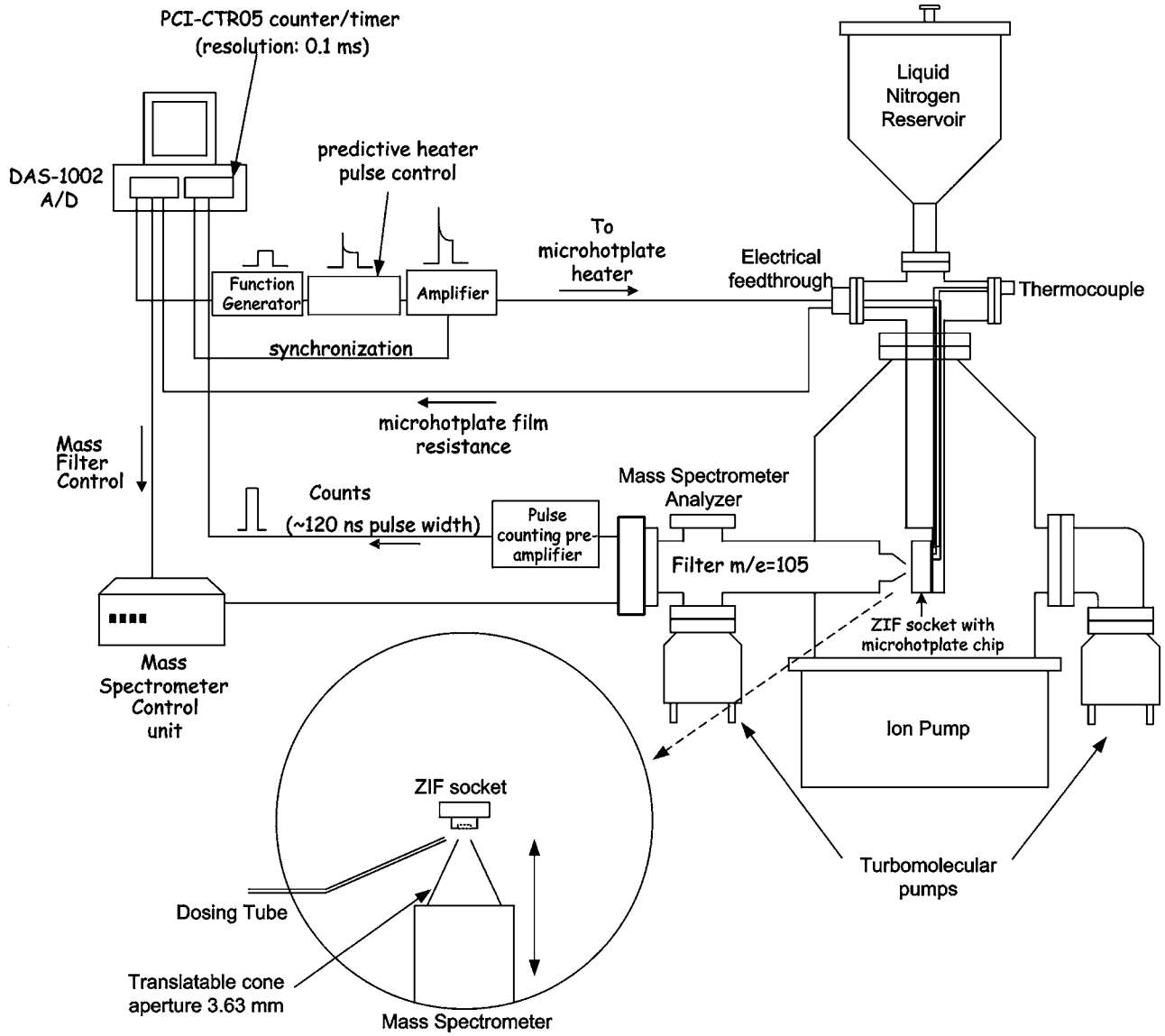

FIG. 2. Schematic of apparatus and electronics for isothermal TPD on microhotplate sensors. The microhotplate sensor is mounted in a zero insertion force (ZIF) socket on a liquid nitrogen cooled probe and positioned within 1 mm of the mass spectrometer cone. The sample is exposed to gases by a directed dosing tube.

and second order desorption models to estimate the kinetic constants for desorption of benzoic acid from a SnO_2 microsensor.

II. EXPERIMENTAL TECHNIQUE

A. Vacuum system

The calibrated thermal desorption system (CTDS),[22] shown in Fig. 2, was modified for the isothermal TPD experiments. The ultrahigh vacuum system is equipped with a differentially pumped, calibrated mass spectrometer, sputtering gun, concentric hemispherical electron energy analyzer, microchannel capillary array doser, dual-anode x-ray source, and a differentially pumped ultraviolet lamp. The main chamber is pumped with a turbomolecular pump and an ion pump and has a base pressure of 2×10^{-8} Pa. A modified mass spectrometer (Balzers QMG 112) assembly resides in a cylindrical shroud, which is coaxial with the ionizer and the quadrupole. The shroud inlet is an x-axis translatable cone with a 3.63 mm diameter aperture to allow entry of the species into the section that is differentially pumped by a second turbomolecular pump. A schematic drawing of the dosing and mass spectrometer arrangement is shown in the inset of Fig. 2. The shroud was designed[22] to meet the following criteria: (a) achieve a linear relationship between the pressure in the ionizer and the mass spectrometer over four orders of magnitude, (b) possess sensitivity to a flux of 10^{10} molecules/cm^2 s, (c) provide a pumping time constant of about 6 ms for inert gases, and (d) have a "pumping speed immunity" or weak dependence of the ionizer region pressure to changes in the pressure at the turbopump inlet.

The CTDS was modified with a directed dosing tube and sample manipulator for measuring the desorption kinetics on the microhotplate sensors. Liquid nitrogen cooling of the

sensors is facilitated by a reservoir connected to the sample manipulator. The *x*-*y* translatable manipulator consisted of a hollow oxygen-free high conductivity copper tube (for liquid nitrogen) extending into the chamber, onto which a zero insertion force (ZIF) socket was mounted to hold the ceramic sensor chip package. A *K*-type thermocouple was spot welded to one of the legs of the sensor chip for measurement of the package temperature. A cylindrical shroud around the ZIF socket with an aperture for access to the sensors was used to limit heating by radiation during adsorption and desorption. The minimum temperature of the microhotplates was approximately 215 K when the probe was liquid nitrogen cooled.

B. Data acquisition and control electronics

A schematic drawing of the data acquisition and control arrangement is also shown in Fig. 2. The electrical connections to the individually addressable components of the microhotplate were made using a 20-pin electrical feedthrough connected to the manipulator. The data acquisition system was configured for pulse counting with an FT-100 preamplifier-discriminator (Advanced Research Instruments) connected to a PCI-CTR05 countertimer card (ComputerBoards Inc.). A DAS 1002 analog-to-digital (A/D) card (ComputerBoards Inc.) controlled the mass spectrometer and triggered a function generator (Sony Tektronix AFG310) to output a square voltage pulse for the microhotplate heater. The A/D card was also configured to measure the film resistance during the desorption experiment. The data acquisition program was written in SoftWIRE™ and Visual Basic to control the DAS 1002 and the PCI-CTR05 boards.

It is possible to measure the electrical resistance of either the polysilicon heater or the sensing film on the surface and correlate the value to surface temperature. The microhotplates have a first order heating time constant, τ_h, of approximately 3 ms for a step change in voltage so the minimum value of the first order desorption time constant that could be measured was about 30 ms without accounting for the heating rate. This heating rate limitation is further discussed in Sec. III B. To enable the measurement of higher desorption rates, a predictive temperature control method was devised as illustrated in Fig. 3. The function generator in the system description was used to create a square voltage pulse of approximately 1 V, which was fed to a circuit designed to create an initial spike in the voltage that decays exponentially to the final voltage value. The signal was then amplified so that the maximum in the initial spike was approximately 25 V, as shown in Fig. 3.

This method of temperature control reduced τ_h to approximately 0.2 ms. The temperature of the microhotplate was determined by heating the package in a tube furnace and correlating the resistance of the embedded heater to the furnace temperature. Then, these temperatures were correlated to the semiconducting SnO_2 film resistance in UHV (without any gas present) because the resistance of the SnO_2 was found to be more sensitive to temperature than the polysilicon heater. It was assumed that the SnO_2 film on the surface

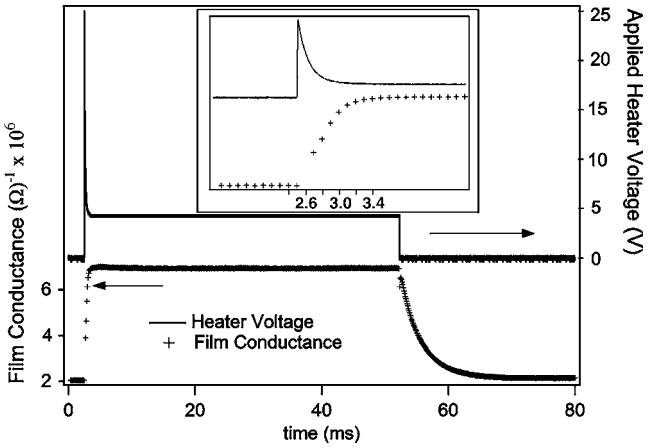

FIG. 3. Tin oxide film conductance response (as a relative measure of surface temperature) to heater voltage pulse without dosing. The ultimate temperature during the applied voltage is 650 K. The initial spike in the applied voltage (predictive temperature control) results in a first order heating time constant of approximately 0.2 ms on the rising edge of the heater pulse. The natural first order cooling (and heating) time constant of the microhotplate to a step change in applied voltage is approximately 3 ms and is characterized by the falling edge at around 50 ms. The rapid heating response to the modified control voltage allows measurement of higher desorption rates.

was at the same temperature as the heater, which is reasonable since there is no heat conduction to the atmosphere in vacuum. The film resistance was measured applying a bias of 5 V across the film and a 10 kΩ reference resistor in series. The electrical current through the film was calculated from the reference voltage measured by the DAS 1002, and this current was used along with the film voltage to calculate the film resistance. This setup allows reliable measurement of the resistance at a time resolution as small as 100 μs. The conductance of the film, G, is proportional to its temperature. The voltage pulse applied to the heater and the film conductance response can be seen in Fig. 3.

The increase in the film conductance at the leading edge of the heating pulse in Fig. 3 is much faster than the decrease at the falling edge. With the predictive temperature control, the temperature of the film reaches steady state in approximately 1 ms and fits τ_h=0.2 ms. To compare the effectiveness of the heating technique, note that the cooling rate when the power is turned off corresponds to a time constant of 3 ms. The speed of the film's electrical response discussed here may be compared with the thermal response observed by Afridi *et al.* with infrared imaging techniques, where the microhotplate reached a steady state temperature within 2 ms.[27]

The desorption signal was measured with the mass spectrometer in pulse-counting mode to maximize the ratio of signal to noise. The pulse-counting preamplifier converts the signal from the multiplier for each detected ion into a 120 ns wide voltage pulse that is detected by the countercard. The countercard uses three AMD9513 counters, two of which were used in cascaded mode to count the 120 ns pulses, and the third for synchronization with the heating pulse. The counters were programmed to integrate for 0.1 ms. The graphing software IGOR PRO 5 (Wavemetrics) was used to fit

the experimental data to the model derived in Sec. III by optimizing the values for τ_{des} and τ_p.

C. Dosing and desorption procedure

The SnO_2 film was cleaned by three oxidation and reduction cycles at 650 K prior to the dosing and desorption experiments. The oxidation procedure consisted of heating the surface in 266 Pa of O_2 for 30 min at 650 K, while the reduction procedure consisted of heating in vacuum at 650 K for 30 min. A 650 K pulse was applied to the heater to desorb any surface impurities at the start of each experiment. Spectroscopic verification of the surface oxidation state and level of contamination was not possible, but was similar to procedures used previously on macroscopic samples.[18]

The experiment consisted of adsorbing benzoic acid on the microhotplate at $T \approx 215$ K, rapidly heating the microhotplate to a high temperature and desorbing the benzoic acid, and monitoring the desorption peak with a quadrupole mass spectrometer. Precise alignment of the mass spectrometer shroud cone was necessary to collect the maximum number of molecules desorbing from the microhotplate during the heating pulse. The cone was moved in to within 1 mm of the microhotplate prior to the application of the heating pulse. The microhotplate chip had four sensors; two with SnO_2 films, and two with TiO_2 films. However, all measurements were conducted on one of the SnO_2 sensors. The dosing apparatus consisted of a glass tube connected to the main chamber by a 6.4 mm outer diameter stainless steel tube via a leak valve. The stainless steel dosing tube extended into the chamber to within 2 cm of the sensor chip. The benzoic acid (99.5%, Aldrich Chemical Co.) was purified by warming it with a hot air gun while pumping on the glass tube with a turbomolecular pump. The crystals sublimed and then condensed on the cooler parts of the tube, releasing trapped water and air in the process.[24,25] The procedure for the benzoic acid desorption consisted of cooling the sensor to about 215 K, applying a 650 K clearing pulse, dosing the benzoic acid at 215 K for 120 min, and then applying a 500 ms long heating pulse to the microhotplate and measuring the film resistance with the DAS 1002 A/D board while collecting the mass spectrometer signal ($m/z=105$ for the major fraction of benzoic acid) from the pulse-counting discriminator. Dosing intervals of 15, 30, 60, 120, and 180 min were used to decide the optimum dosing time, and the desorption signal was found to have reached its maximum within 120 min. Benzoic acid could be desorbed while dosing, and the time required for saturation of the signal was independent of the amount of time that the dosing valve had been open, suggesting that dosing was not limited by the time for the dosing system to reach steady state flux. The base pressure in the system was 6×10^{-8} Pa. The background pressure of benzoic acid during dosing was about 4×10^{-8} Pa, resulting in an estimated dose of greater than 2×10^{15} cm^{-2} because of the directed dosing arrangement. We expected benzoic acid to have a sticking probability of almost unity.[28] However, our estimate for the number of desorbed molecules is only 10^8, suggesting a much lower sticking probability.

III. THEORETICAL FRAMEWORK

A. Desorption model

The desorption kinetics can be measured without the influence of system pumping effects only when the desorption time constant is much larger than the pumping speed and heating rate time constants. A first order process model is developed in the following discussion to account for the desorption rate, the pumping speed, and the heating rate of the microhotplate. Although the concepts of thermal desorption have been well known for years, particularly in temperature ramp experiments,[10–12,14–20] the current model is unique since it develops a closed-form solution for the general, isothermal desorption case when the pumping time constant and the desorption time constant may be of comparable magnitude and neither can be neglected.

Consider the volume of the mass spectrometer shroud, which the desorbing molecules enter through the conical opening. A molecule balance on the shroud volume gives the following relationship:

$$\frac{dN}{dt} = r_{\mathrm{des}} - S\frac{N}{V}, \tag{1}$$

where dN/dt is the rate that molecules accumulate in the shroud (molecules/s), r_{des} is the rate that desorbing molecules enter the shroud (molecules/s), S is the pumping speed of the shroud (m^3/s) and N/V represents the molecular concentration in the shroud volume (molecules/m^3). To write Eq. (1) in terms of the pressure in the shroud, we use the ideal gas law as follows:

$$N = P\left(\frac{V}{k_B T_B}\right) = P\left(\frac{1}{A}\right), \tag{2}$$

where k_B is Boltzmann's constant, T_g is the gas temperature in the shroud, and A is a convenient grouping of constants: $k_B T_g/V$. Then Eq. (1) becomes

$$\frac{d(P/A)}{dt} = r_{\mathrm{des}} - \frac{S}{V}\frac{P}{A} \tag{3}$$

and defining a characteristic pumping time constant, τ_p, as

$$\tau_p = \frac{V}{S} \tag{4}$$

then the first order differential equation relating the shroud pressure to the desorption rate is

$$\frac{dP}{dt} + \frac{P}{\tau_p} = A r_{\mathrm{des}}. \tag{5}$$

The desorption rate is a function of surface coverage and, therefore, varies during the isothermal TPD experiment. The model at this point is completely general.

The intensity of the mass spectrometer signal (counts/s) was calibrated by calculating the flow of benzoic acid into the shroud based on the background pressure of benzoic acid in the chamber during dosing. The flow of molecules into the shroud was used to determine a proportionality constant relating the shroud pressure to signal intensity. The flux of molecules impinging the shroud aperture Γ[molecules/cm^2 s] is

$$\Gamma = \frac{P_{\mathrm{CTDS}}}{\sqrt{2\pi m k_B T_g}}, \tag{6}$$

where P_{CTDS} is the partial pressure of benzoic acid in the chamber, m is the molecular mass, and k_B is the Boltzmann constant. The flow of molecules into the shroud is the product of Γ and the aperture area, A_{aperture}, so from Eq. (5) with r_{des} replaced with the flow, the steady state pressure in the shroud is then

$$P = A\tau_p \Gamma A_{\mathrm{aperture}}, \tag{7}$$

and the signal intensity is

$$I = \alpha\tau_p \Gamma A_{\mathrm{aperture}}, \tag{8}$$

where α is the product of A and a proportionality constant relating pressure to signal intensity. Therefore all equations in terms of pressure can easily be transformed to terms of intensity by replacing P with I and replacing A with α. The partial pressure of benzoic acid in the chamber, P_{CTDS}, was approximately 4×10^{-8} Pa during dosing, so the flux of benzoic acid was 5×10^{10} molecules/cm^2 s. The intensity of the peak for m/z=105 was 6.5×10^5 counts/s, the circular aperture diameter is 3.6 mm, and we will show later that $\tau_p \approx 6$ ms. Therefore the value of α was estimated to be 0.02 counts/s per benzoic acid molecule.

Next, we adapt Eq. (5) for zero, first, and second order desorption kinetics. The rate of desorption from a surface with N_S molecules is

$$r_{\mathrm{des}} = -\frac{dN_S}{dt} = k_n N_S^n, \tag{9}$$

where n is the desorption order and k_n is a temperature-dependent rate constant that we will assume follows the Arrhenius form

$$k_n = \nu e^{-E_{\mathrm{des}}/RT}, \tag{10}$$

in which ν is the prefactor, E_{des} is the activation energy for desorption, R is the ideal gas constant, and T is the surface temperature. We consider the cases of zero, first, and second order desorptions, and show that their functional forms offer the possibility of determining the order of simple processes from the data. This is in contrast to temperature ramp TPD, in which the order is assumed prior to data analysis.

Zero order desorption (multilayer). For the case of zero order kinetics (n=0), the rate of desorption is

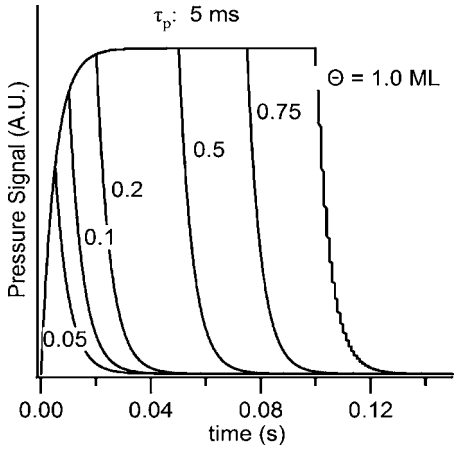

FIG. 4. Modeled signal response for zero order isothermal desorption. The signal abruptly decreases when all adsorbed molecules have desorbed, and this occurs at a later time as coverage (θ) increases. The curves are shown for coverages ranging from 0.05 to 1.0 ML.

$$r_{\mathrm{des}} = -\frac{dN_s}{dt} = k_0 \quad \text{for } t \leqslant t_N, \tag{11}$$

where t_N represents the time at which the last molecule desorbs.

The differential equation for zero order kinetics relating pressure to desorption rate is then

$$\frac{dP}{dt} + \frac{P}{\tau_p} = Ak_0, \tag{12}$$

which yields

$$P(t) = Ak_0\tau_p(1 - e^{-t/\tau_p}) \quad (t \leqslant t_N). \tag{13}$$

After all molecules have desorbed, the right side of Eq. (12) is zero and

$$P(t) = Ak_0\tau_p(e^{t_N/\tau_p} - 1)e^{-t/\tau_p} \quad (t > t_N). \tag{14}$$

The time t_N may be derived by integrating Eq. (11) to obtain

$$t_N = \frac{N_{S,0}}{k_0}. \tag{15}$$

Figure 4 shows the calculated pressure signal for zero order desorption for a range of surface coverage. Both the rising and falling time constants are determined by τ_p, and during a steady state condition, the pressure is independent of coverage.

First order desorption. Integrating Eq. (9) for first order desorption (n=1) from a surface with initially $N_{S,0}$ molecules yields

$$N_S(t) = N_{S,0}e^{-k_1 t}. \tag{16}$$

The number of molecules that have desorbed at time t is then given by $N_{\mathrm{des}}(t)$,

$$N_{\mathrm{des}}(t) = N_{S,0} - N_S(t) \tag{17}$$

and substituting Eq. (16) into Eq. (17) and differentiating yield the time dependent desorption rate

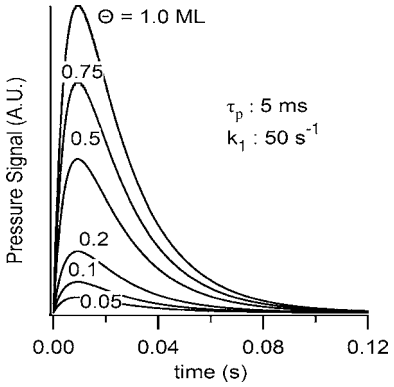

FIG. 5. Modeled signal response for first order isothermal desorption. The curves are modeled using a τ_p of 5 ms, and a τ_{des} of 20 ms for coverages (θ) ranging from 0.05 to 1.0 ML. The time of the peak maximum is independent of coverage.

$$r_{\mathrm{des}} = \frac{dN_{\mathrm{des}}(t)}{dt} = N_{S,0} k_1 e^{-k_1 t}. \tag{18}$$

As with the pumping time constant, a characteristic time constant for desorption can be defined as

$$\tau_{\mathrm{des}} = \frac{1}{k_1}. \tag{19}$$

Now Eq. (5) can be written as

$$\frac{dP}{dt} + \frac{P}{\tau_p} = A \frac{N_{S,0}}{\tau_{\mathrm{des}}} e^{-t/\tau_{\mathrm{des}}} \quad (n=1), \tag{20}$$

which may be solved analytically using Laplace transforms or an integrating factor, and the solution is given by

$$P = A N_{S,0} \left(\frac{\tau_p}{\tau_p - \tau_{\mathrm{des}}} \right) (e^{-t/\tau_p} - e^{-t/\tau_{\mathrm{des}}}) + P_0 \quad (n=1). \tag{21}$$

To compare the modeled pressure with the signal intensity from the experimental data, using Eqs. (7) and (8), Eq. (21) may be written as

$$I = \alpha N_{S,0} \left(\frac{\tau_p}{\tau_p - \tau_{\mathrm{des}}} \right) (e^{-t/\tau_p} - e^{-t/\tau_{\mathrm{des}}}) + I_0 \quad (n=1), \tag{22}$$

where I_0 is the background signal intensity.

For the special case of $\tau_p = \tau_{\mathrm{des}} = \tau$, the solution to Eq. (20) is given by

$$P = \frac{A N_{S,0} t}{\tau} e^{-t/\tau} + P_0 \quad (n=1). \tag{23}$$

Figure 5 shows the calculated pressure signal for first order desorption for various coverages. Notice that the peak time is independent of coverage.

The predicted effects of the desorption and pumping time constants on the pressure response are shown in Figs. 6 and 7 for the first order desorption case using parameters typical of our experimental system. For the case of benzoic acid on a SnO_2 microhotplate, no desorption signal could be detected for desorption temperatures below approximately 300 K. At this temperature, desorption occurs over a time on the order of 1000 ms, and it is desirable to measure desorption rates spanning a few orders of magnitude so that kinetic parameters can be determined. Therefore, the maximum desorption rates would occur on a 1 ms time scale which is comparable to the 6 ms pumping time constant measured for the CTDS system. We show the simulated mass spectrometer signal as a function of these parameters for first order desorption assuming an instantaneous temperature step. For $\tau_{\mathrm{des}} = 1$ ms, Fig. 6 illustrates how the signal intensity initially increases with increasing τ_p because the molecules reside in the ionizer longer. However, as τ_p increases further ($\tau_p > 10\tau_{\mathrm{des}}$), the signal saturates and the decay of the signal is controlled by the pumping speed. Decreasing τ_{des} for $\tau_p = 10$ ms also increases the signal response, as shown in Fig. 7, where $\tau_p = 10$ ms was chosen since the characteristic pumping time constant of the CTDS system for noble gases is of the same order of magnitude. The effects of extremely slow pumping can be seen in Fig. 6, while Fig. 7 shows how the time

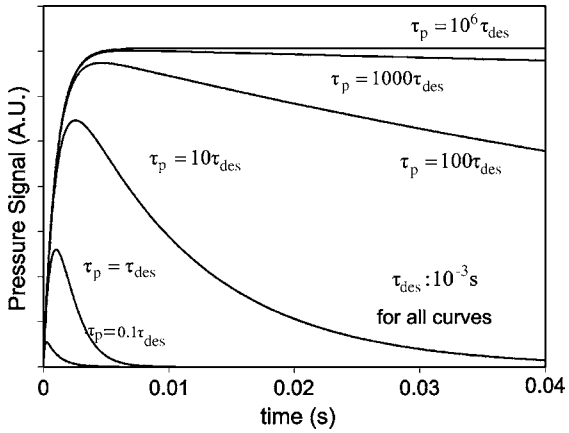

FIG. 6. Modeled signal response to varying τ_p for constant τ_{des}. For large $\tau_p / \tau_{\mathrm{des}}$ the signal decay is controlled by the pumping speed. The molecules reside in the chamber longer and the signal saturates. As τ_p approaches τ_{des}, the signal is influenced by both the desorption and pumping rate constants.

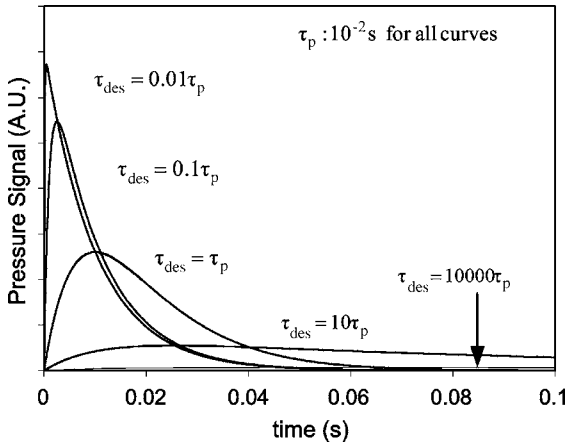

FIG. 7. Modeled signal response to varying τ_{des} for constant τ_p. When $\tau_{\mathrm{des}} \ll \tau_p$, the decay of the signal is represented by τ_p. As τ_{des} approaches τ_p, the rise and decay are influenced by both τ_{des} and τ_p and neither can be determined independently.

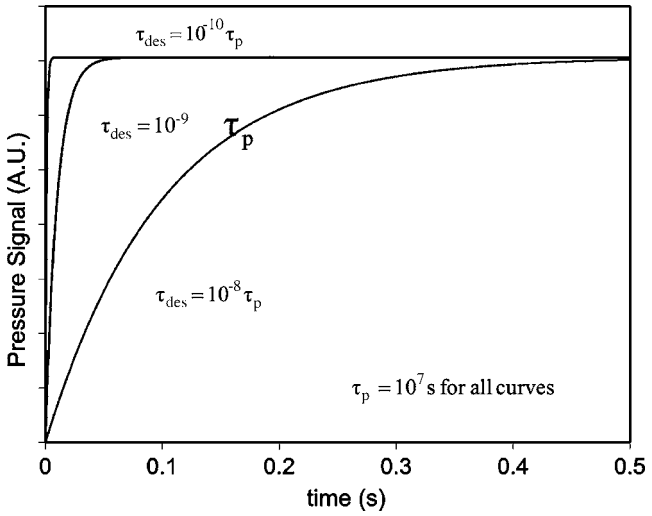

FIG. 8. Modeled pressure signal for the pumping controlled regime. For $\tau_p \gg \tau_{\text{des}}$ as described by Eq. (26) in the text. The asymptotic increase of the signal is independent of τ_p and only depends on τ_{des} in this extreme.

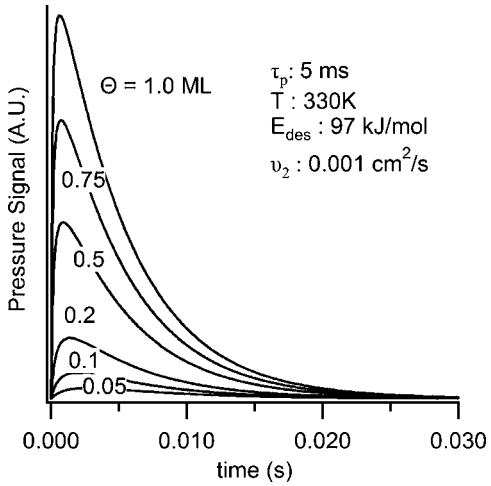

FIG. 9. Modeled signal response for second order isothermal desorption. The curves are modeled using a τ_p of 5 ms, a surface temperature of 330 K, an activation energy of 97 kJ/mol, and a prefactor of 0.001 cm^2 s^{-1}, for coverages (θ) ranging from 0.05 to 1.0 ML. The peak maximum shifts to earlier times as coverage increases.

dependent signal will evolve as the isothermal desorption temperature increases (i.e., τ_{des} decreases) for a fixed pumping time constant.

The desorption time constant can be determined directly from the system response in the extremes of both relatively fast and relatively slow pumping. For the case of relatively fast pumping ($\tau_p \ll \tau_{\text{des}}$), Eq. (21) is simplified to

$$P \approx AN_{S,0}\left(\frac{\tau_p}{\tau_{\text{des}}}\right)e^{-t/\tau_{\text{des}}} + P_0 \quad (n=1, \tau_p \ll \tau_{\text{des}}). \tag{24}$$

By substituting Eqs. (18) and (19) into Eq. (24), the model predicts the pressure to be proportional to the rate of desorption as was the case in the work of DeAngelis and Anton,

$$P \approx A\tau_p r_{\text{des}} + P_0 \quad (n=1, \tau_p \ll \tau_{\text{des}}). \tag{25}$$

For the case of relatively slow pumping ($\tau_p \gg \tau_{\text{des}}$), Eq. (21) simplifies to

$$P \approx AN_{S,0}(1 - e^{-t/\tau_{\text{des}}}) + P_0 \quad (n=1, \tau_p \gg \tau_{\text{des}}). \tag{26}$$

Performing a desorption experiment without pumping the mass spectrometer (in our case, by closing the gate valve to isolate the mass spectrometer from the turbomolecular pump) may thus provide the desorption time constant even for a pumping limited situation. The dependence of the modeled asymptotic pumping signal on the desorption time constant is evident in the rise time of the curves in Fig. 8.

Second order desorption. For the case of second order desorption, the rate equation may be written as

$$r_{\text{des}} = -\frac{dN_S}{dt} = k_2 N_S^2 \quad (n=2). \tag{27}$$

On integrating Eq. (27) with the initial condition of $N_S = N_{S,0}$ at $t=0$, we obtain

$$N_S(t) = \frac{N_{S,0}}{(k_2 N_{S,0} t + 1)} \quad (n=2). \tag{28}$$

Equation (5) for the second order case then yields

$$\frac{dP}{dt} + \frac{P}{\tau_p} = \frac{Ak_2 N_{S,0}^2}{(k_2 N_{S,0} t + 1)^2} \quad (n=2). \tag{29}$$

The analytical solution obtained by using an integrating factor is given by

$$P(t) = e^{-t/\tau_p}(f(t) - f(0)) \quad (n=2), \tag{30}$$

where

$$f(t) = \frac{A}{\tau_p k_2}\left[-\frac{\tau_p k_2 N_{S,0} e^{t/\tau_p}}{(k_2 N_{S,0} t + 1)} + e^{-1/\tau_p k_2 N_{S,0}}\,\text{Ei}\left(\frac{(k_2 N_{S,0} t + 1)}{\tau_p k_2 N_{S,0}}\right)\right] \quad (n=2). \tag{31}$$

The exponential integral Ei(x) is

$$\text{Ei}(x) = \int_{-\infty}^{x} \frac{e^u}{u} du \quad (x > 0). \tag{32}$$

Figure 9 shows the effect of coverage on the desorption signal for second order desorption. Notice that the peak time decreases as the coverage increases.

B. Effect of system constraints on desorption kinetics measurements

1. Comparison of zero, first, and second order kinetics

There are several ways to distinguish the order of desorption from isothermal desorption data. A comparison of the theoretical zero, first, and second order desorption spectra shows that zero order kinetics predicts distinctly different desorption characteristics when compared to first and second

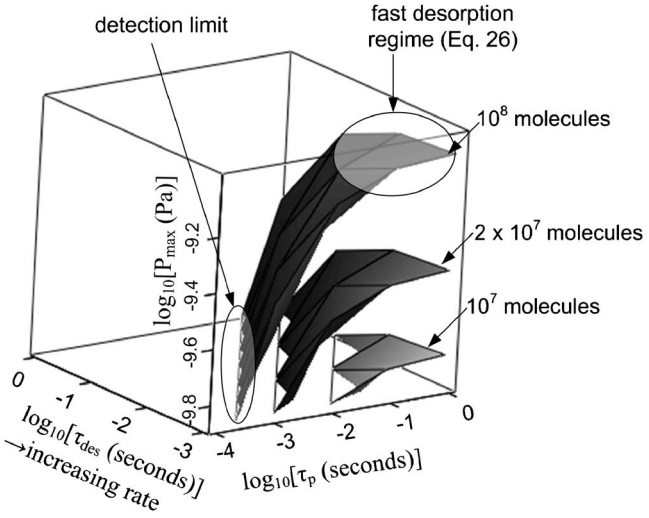

FIG. 10. Dependence of the peak desorption pressure (i.e., desorption rate in the fast heating limit) on the desorption and pumping time constants for the indicated number of molecules, as simulated using Eq. (21) in the text. The time constants must be chosen such that the desorption signal is above the detection limit of the mass spectrometer (chosen to be $P=10^{-10}$ Pa for our instrument) but below the point at which the signal saturates in the slow pumping limit. With our system, which was designed for a pumping time constant of 6 ms, the isothermal desorption temperature can be varied over a sufficiently large range to quantify the desorption parameters (desorption energy and preexponential factor) for 10^8 molecules.

order desorption spectra which are more similar to each other. For zero order desorption, the exponential rise and fall time constants are equal to τ_p and so the dynamics contain no information regarding k_0. This information is only contained in the magnitude of the plateau at high coverages. First and second order desorption spectra can be distinguished if experiments can be conducted with varying surface coverage, since the peak time shifts for second order but not first. Alternatively, with sufficient signal-to-noise ratio, the time dependent signals can be distinguished because the tail of the desorption spectrum persists longer for second order. By fitting a desorption spectrum to first and second order models, the quality of the fits can be evaluated by comparing chi-squared values for each model. Arrhenius analysis can be done for a set of desorption spectra at different temperatures using fits to both first and second order models. The relative linearity of the two plots may indicate that one model is preferred over the other. Also, with a calibrated system, the initial coverage can be determined from the area under the desorption curve, which allows us to calculate the second order prefactor. The reasonableness of the prefactors that are obtained through the Arrhenius analyses can then be compared with transition state theory and literature values.

2. Sensitivity and detection limits

Measuring a desorption signal from a single microhotplate requires high instrument sensitivity, and high desorption rates because of the low total molecular surface coverage on a 10^{-4} cm^2 device. To predict the regime in which a desorption signal can be measured, we constructed the three-dimensional plot in Fig. 10 which quantifies how the peak desorption pressure for a first order desorption pulse (like those in Fig. 6) vary with the desorption and pumping time constants for different initial coverages. Equation (21) was used to predict the maximum desorption pressure for a range of τ_{des} and τ_p in the limit of $\tau_h=0$. The value of $N_{S,0}=10^8$ molecules represents 0.1% of a monolayer on the sensing film as predicted by the Weisz model, which is a conservative estimate. The instrument sensitivity and signal-to-noise ratio determine the limit of detection. The lowest measurable pressure for our mass spectrometer is 1×10^{-10} Pa, and that imposes a limit in the form of the bottom plane of the plot in Fig. 10. The lower limit of $\tau_{\mathrm{des}}=1$ ms was chosen because of heating rate limitations which will be discussed in the next section. Increasing the desorption rate (i.e., increasing the isothermal desorption temperature, which decreases τ_{des}) improves the sensitivity. However, when τ_{des} is much smaller than τ_p, the initial height of the peak is proportional to the number of molecules that "instantaneously" desorbed, and the shape of the curve is independent of τ_{des}. The surfaces for lower values of $N_{S,0}$, down to 10^7 molecules, lie above the 10^{-10} Pa detection limit, but they are in the relatively fast desorption regime and offer no estimate for the desorption time constant. So, τ_{des} and τ_p must be chosen such that the peak desorption signal is greater than the detection limit (i.e., $P_{\max}>P_{\mathrm{det}}$), but still in the fast desorption regime ($\tau_p \leqslant \tau_{\mathrm{des}}$). In principle, if τ_p could be varied along with the desorption temperature, optimal conditions (with the signal near the top of the steep surface) could be maintained to give the best signal-to-noise ratio at all temperatures. In our system the pumping time constant was not variable. Nevertheless, it is remarkable to be able, as we will show, to detect and quantify the desorption parameters from such a low quantity of adsorbates (10^8 molecules or 1 fmol).

The model can be used to estimate the bounds of the operating space in which desorption kinetics can be studied for a particular mass spectrometer detection limit. The calculated maximum in the desorption signal is shown in Fig. 10 for three initial coverages assuming all desorbing molecules enter the mass spectrometer shroud. The lowest pressure in Fig. 10 represents our estimated lower detection limit, and ideally, a pumping time constant less than one-tenth of the desorption time constant is desired and that defines a narrow region in the time constant x-y plane.

3. Heating rate limitations

The pressure response model developed in Eq. (21) assumes the heating rate is much greater than the desorption rate. The limits of heating rate can be explored by approximating the microhotplate's response, $T(t)$, to a step change in heater voltage as a first order process

$$T(t) = T_f - (T_f - T_i)e^{-t/\tau_h}, \tag{33}$$

where T_f and T_i are the final and initial temperatures of the sensor, and τ_h is a characteristic heating rate constant. The time-varying desorption rate constant is then

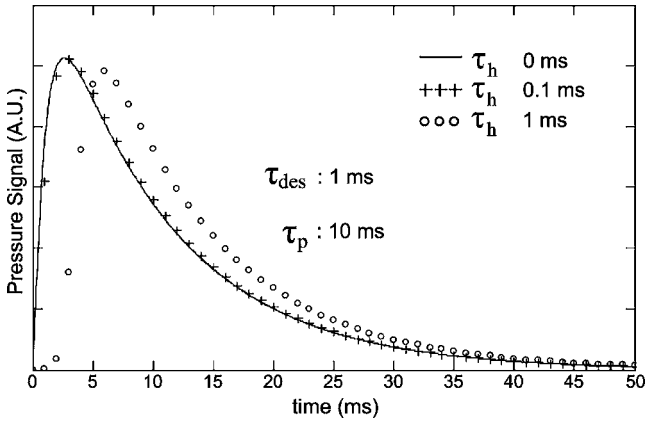

FIG. 11. Effect of τ_h on the desorption kinetics as it approaches τ_{des} for a range of heating rates and for $\tau_p=10$ ms and $\tau_{\text{des}}=1$ ms. When τ_h is less than 10% of τ_{des}, the signal is almost identical to that for the ideal case where τ_h is zero. As τ_h approaches τ_{des}, the shape of the desorption curve changes and is accompanied by an initial temporal offset.

$$k_n(t) = \nu e^{-E_{\text{des}}/R(T_f-(T_f-T_i)e^{-t/\tau_h})}, \tag{34}$$

which was used along with Eqs. (19) and (20) to predict a pressure response for a first order process. The equations were solved numerically for $E_{\text{des}}=122$ kJ/mol, $\nu=10^{13}$ s^{-1}, and a range of τ_h. E_{des} was chosen so that $\tau_{\text{des}}=1$ ms at $T_f=650$ K and $T_i=210$ K. The results are presented in Fig. 11. The case for no heating rate limitation is represented by the curve for a $\tau_h=0$ ms. As shown in Fig. 11, a small temporal offset ($\approx 3\tau_h$) is observed when τ_h is within an order of magnitude of the desorption rate constant, and τ_h does not affect the shape and height of the desorption curve when it is ten times smaller than τ_{des}. We have used these criteria in restricting the range of desorption temperature for analysis of the data, so that we could use analytical expressions in the curve fitting process and obtain estimates of the uncertainties in the parameters. It would be possible to solve the full, three parameter (τ_{des}, τ_p, and τ_h) differential equations numerically, which would extend the range but increase the complexity of error analysis.

IV. RESULTS AND DISCUSSION

Isothermal desorption measurements were made for temperatures ranging from 296 to 347 K, and the results are shown in Fig. 12. Comparison of the shapes of the curves for the zero, first, and second order desorption models in Figs. 4, 5, 7, and 9 to the data indicate that desorption might be either first or second order. We believe the desorption data are best represented by first order kinetics based on a number of criteria. These include goodness of fit, as well as the reasonableness of the calculated kinetic parameters. Therefore, we will first discuss how the data were analyzed using our first order model, present the results from a similar analysis using the second order model, and then compare the important facts which rule out second order kinetics.

The first order time constants were determined at each temperature by fitting the desorption curve with the modeled curve. The fitted curves are presented along with the experimental data in Fig. 12. The value of τ_p ranged from 4 to 7 ms. The confidence intervals for the τ_p values ranged from 1 to 6 ms, with the larger relative uncertainties for

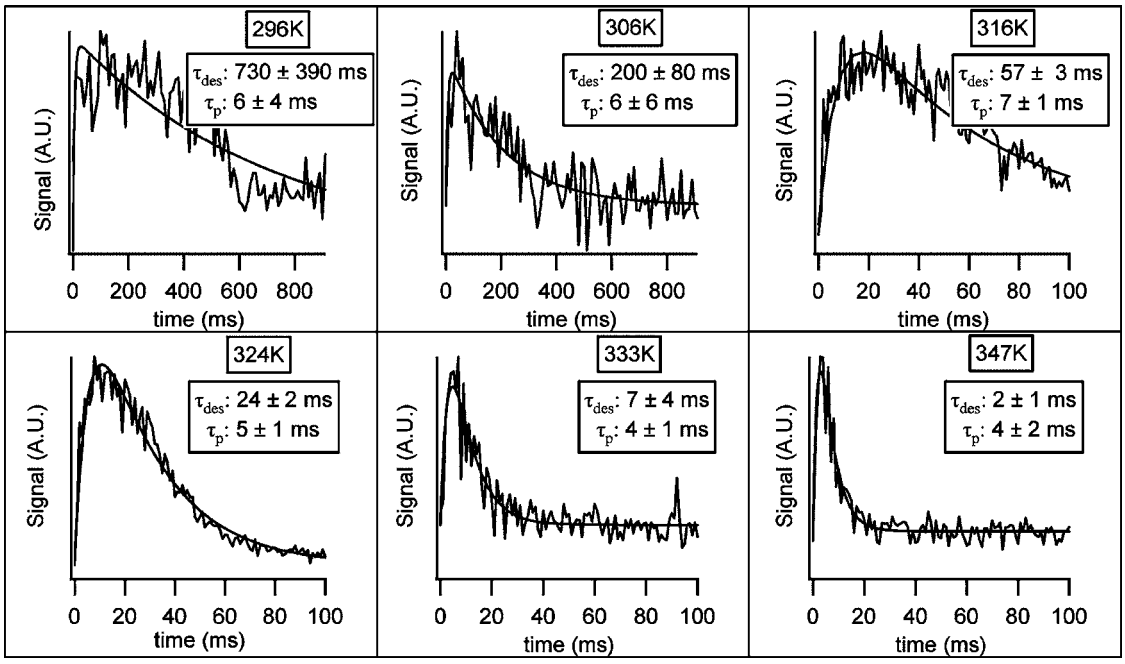

FIG. 12. Comparison of model and experiment desorption curves for different surface temperatures for desorption of benzoic acid on a SnO_2 microsensor with nominal surface area of 10^{-4} cm^2. Surface temperatures range from 296 to 347 K from top left to bottom right. Equation (21) was used to predict the best values of τ_{des} and τ_p for the data and the shapes of the desorption curves are similar to those simulated in Figs. 6 and 7. The data fit τ_p values in the range of 4–7 ms. The higher relative uncertainties in τ_{des} near the lowest surface temperature were due to the low signal-to-noise ratio, while those near the highest temperature were due to the limit of the sampling resolution.

curves near 300 K. To obtain an independent estimate of the pumping time constant, desorption at 650 K was also measured, since the desorption time constant at this temperature was much smaller than the pumping time constant, and as a result, the curvature of the desorption signal was dominated by τ_p. The value of τ_p determined from the 650 K desorption was 5 ms. The observed variation in fitted τ_p may have resulted from changes in shroud temperature, which could affect the sticking of benzoic acid on surfaces in the mass spectrometer. Indeed, the pumping time constant has been observed to increase after long periods of operating the mass spectrometer ionizer. Therefore, the ionizer was only operated for 5 min periods prior to conducting desorption experiments. The data were integrated for 1 ms intervals to reduce computation since the heating time constant limited our measurements to $\tau_{\text{des}} > 2$ ms.

The desorption curves obtained from the experiment qualitatively resemble those predicted by the first order model for the various regimes of τ_{des} shown in Fig. 7 as the surface temperature was increased. The desorption curve for 296 K fits $\tau_{\text{des}}=730\pm390$ ms, the curve for 306 K fits $\tau_{\text{des}}=200\pm80$ ms, and desorption for 316 K fits $\tau_{\text{des}}=57\pm3$ ms. The 324 K desorption has a $\tau_{\text{des}}=24\pm2$ ms, the 333 K data have a $\tau_{\text{des}}=7\pm4$ ms, and the 347 K data fit $\tau_{\text{des}}=2\pm1$ ms. At the lower surface temperatures, the lower signal-to-background ratio contributes to the larger uncertainties in τ_{des}. The smallest uncertainties are observed for the mid-range temperature values between 306 and 325 K. The higher-temperature desorption curves have shorter tails with higher peaks, consistent with the rapid desorption of the adsorbed molecules. The relative uncertainties increase again at the higher temperatures, where τ_{des} is comparable to τ_p. Since the desorption time constant is smaller than the pumping time constant, the information related to τ_{des} is primarily contained in the first few milliseconds at the higher temperatures and is limited by the temporal resolution and signal-to-noise ratio. Also, the finite heating rate becomes more important at the higher temperatures which, on the basis of the criteria discussed in the previous section, limits the measurement to temperatures below which τ_{des} is greater than about 2 ms. Therefore, the highest surface temperature used for the kinetic analysis was 347 K, which corresponded to $\tau_{\text{des}} \approx 2$ ms. The analysis of the experimental data using the model also provided an estimate of the number of molecules adsorbed on the surface. The calibration of the signal intensity with pressure in the mass spectrometer shroud enabled the determination of the coverage on the microhotplate surface. The values of $N_{S,0}$ estimated from the first order fits to the data using the calibration factor α, as well as independent estimates of the values obtained by integrating the areas under the desorption curves, ranged from 3×10^7 to 8×10^8 molecules with an average value of 3×10^8 molecules.

An Arrhenius plot of the first order desorption time constants is presented in Fig. 13. The error bars associated with each data point represent the 95% confidence interval for the τ_{des} values. The values of the desorption activation energy and the rate constant prefactor were determined from a

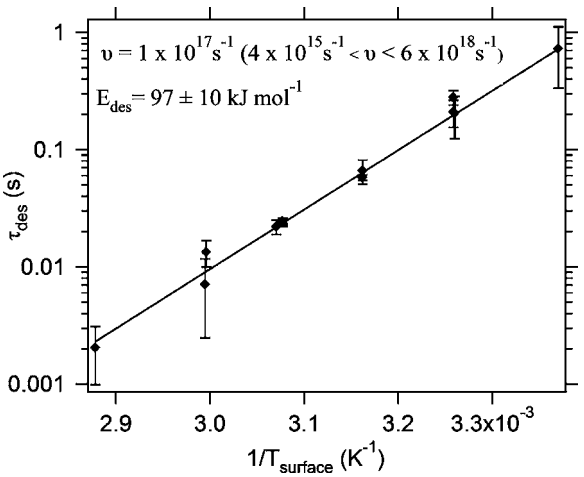

FIG. 13. Arrhenius plot of τ_{des} as a function of $1/T$ for the data in Fig. 12 to determine the prefactor and desorption energy of benzoic acid on the SnO_2 microsensor. At the highest temperature ($\approx$350 K), τ_{des} is ten times τ_h which is the model's lower limit predicted by the results in Fig. 11.

confidence-weighted linear fit to $\ln(\tau_{\text{des}})$ vs $1/T$. The slope and intercept from this analysis are 97 ± 10 kJ/mol and 1×10^{17} s^{-1}, respectively. The 95% confidence interval for the prefactor was estimated to range from 4×10^{15} to 6×10^{18} s^{-1}. The prefactor differs from the commonly assumed value of 10^{13} s^{-1} but a review of preexponential values observed in desorption from metals[29] and semiconductors[30] shows that the distribution of prefactors can vary four orders of magnitude above and below 10^{13} s^{-1} for first order desorption. Thus our results are well within this range for first order desorption. For higher fractional coverage, simple analysis methods can lead to "false" compensation effects, resulting in errors in E_d of 10 kJ/mol and ν_1 by several orders of magnitude. However, Nieskens *et al.* showed that the simple methods work correctly in the limit of zero coverage.[20] Based on our estimate of 10^8 molecules desorbed and a minimum surface area of 10^{-4}cm^2, the fractional coverage is less than 0.005 ML.

The desorption spectra were also fitted to the second order model using techniques similar to those for the first order analysis. An Arrhenius plot of $\ln(k_2)$ vs $1/T$ was nonlinear and gave a desorption energy of 121 ± 65 kJ/mol with a prefactor of 8×10^8 cm^2/s. The 95% confidence interval for the prefactor was estimated to be from 1×10^{-2} to 4×10^{19} cm^2/s. The unreasonably high prefactor from the second order analysis and the nonlinearity of the Arrhenius plots shows that second order desorption kinetics does not fit our experimental data very well. The second order fits for the two surface temperatures which had the lowest uncertainty (324 and 316 K) showed higher chi-squared values than the first order fits, with lower values indicating better quality of fit. In 2001, Lilach *et al.*[31] studied isothermal desorption of N_2 on Ru(001) and demonstrated that a plot of the reciprocal of the square root of the pressure signal $(1/\sqrt{P(t)})$ versus time should be linear for second order desorption with relatively fast pumping speed. Because the method is very sensistive to the choice of base line and our data contain signifi-

cant contributions from the pumping time, this analysis did not clearly distinguish between first and second orders.

The chemistry of benzoic acid was previously studied on other oxides, viz, on $TiO_2(110)$ by Guo *et al.* in 1997,[28] and on powdered ZnO and ZrO_2 by de Lange *et al.* in 2001.[32] Benzoic acid was found to dissociate on reduced $TiO_2(110)$ (1×1) at room temperature to form a bidentate benzoate $p(2\times1)$ and a surface hydroxyl. The adsorbed benzoate was observed to be bound to two Ti^{4+} cations by the oxygens in the benzoate and have an upright surface configuration with the molecular axis perpendicular to the surface. Guo *et al.* noted that annealing the surface to temperatures above 450 K led to the loss of surface hydroxyl and benzoate species most probably by recombinative desorption. de Lange *et al.* observed that benzoic acid was deoxygenated to benzaldehyde at oxygen vacancies on powdered ZnO and ZrO_2 at temperatures ranging from 600 to 700 K. They observed the further slow decomposition of strongly bound benzoates to yield benzene and benzophenone beyond 620 K.

We find no evidence for dissociative chemisorption on SnO_2 in the current study. Instead, we believe we have observed molecular desorption of weakly bound benzoic acid from the SnO_2 film in the 296–347 K range. The calculated desorption energy, within experimental uncertainty, is not significantly larger than the multilayer desorption energy of 91.5 kJ/mol measured for benzoic acid on Cu(110),[26] or the heat of sublimation of benzoic acid, which is 91.2 kJ/mol.[33] If the strength of the molecule-surface interaction is comparable to that of molecule-molecule interactions, then at low coverage ($\theta\leqslant0.005$ ML), we expect the benzoic acid to be adsorbed essentially in the first layer. The observed time dependent curves are consistent with first order desorption with coverage limited to less than a monolayer. If the molecule-surface interaction were weaker than the molecule-molecule interaction and diffusion during adsorption was rapid then multilayer formation would be possible essentially forming three-dimensional islands, even though the total fractional coverage is less than 0.005 ML. Comparing the results in Fig. 12 with the low coverage curves of Fig. 4 our desorption spectra are inconsistent with zero order kinetics. The curves should all have an exponential rise and fall, with the same time constant, $\tau_p\approx6$ ms. At higher temperature [Eq. (13)], the amplitude would be larger, but for the same initial coverage, the time to deplete the surface t_N, would be smaller. The results in Fig. 12 are not consistent with this. Although our calibration gave a fractional coverage much less than one, we know that for coverages larger than one, the *isothermal* desorption spectrum for zero order kinetics would have a plateau where the constant desorption rate would be equal to the pumping rate. Under no conditions do we observe such a plateau in our data.

Our results do not preclude deprotonation to benzoate on the surface as observed by Guo *et al.* on $TiO_2(110)$, but benzoate would have either further decomposed and desorbed as benzaldehyde or other decomposition products or it would have recombined with surface hydroxyls to desorb as benzoic acid. To determine whether there was significant decomposition of benzoic acid on the surface, we compared desorption spectra for $m/z=44$ (CO_2), $m/z=18$ (H_2O), $m/z=122$ (benzoic acid parent molecule), and $m/z=105$ (benzoic acid major fragment and benzaldehyde parent molecule). The relative areas for the $m/z=105$ and $m/z=122$ are consistent with benzoic acid, not benzaldehyde, and there is no evidence for CO_2 or H_2O desorption in this study.

In the study by Ma *et al.*[18] of methanol on WO_3, methanol was observed using ultraviolet photoemission spectroscopy to adsorb molecularly on the oxidized surface, but to dissociate into methoxy and hydroxyls on the reduced surface. However, the desorption kinetics could be modeled using first order kinetics in both cases. They ascribed this to the possibility that the hydroxyl and methoxy groups were not very mobile, and therefore did not have to diffuse around the surface before reacting with each other. Such a process would be consistent with first order desorption, but we have no spectroscopic evidence in support of it.

V. CONCLUSIONS

The technique presented in this work shows how the desorption energy and the preexponential factor can be determined for a model system in ultrahigh vacuum, under conditions where the pumping speed plays an influential role in the observed desorption spectra. The technique makes it possible to characterize the adsorption energy for an analyte on an actual microhotplate gas sensor which has an extremely small surface area and a number of adsorbates (as small as 10^8 molecules) by taking advantage of the extremely large heating rates (up to 10^6 K/s) of microhotplate sensors. Modeling the desorption kinetics in this fashion, while accounting for the pumping and heating rates, can lead to the extraction of the desorption parameters in a straightforward manner, establish the regimes in which a measurable desorption signal may be observed, and provide an estimate of the coverage. Using adsorption of benzoic acid on a SnO_2 sensor, we have demonstrated from the results in Figs. 12 and 13 that it is possible to measure the desorption time constant independently of the pumping time constant in regimes where the two are comparable.

ACKNOWLEDGMENT

This work was supported in part by National Science Foundation Grant No. CTS-0428341.

[1] J. Bryzek, K. Petersen, and W. Mcculley, IEEE Spectrum **31**, 20 (1994).
[2] S. Semancik and R. E. Cavicchi, Acc. Chem. Res. **31**, 279 (1998).
[3] S. Semancik *et al.*, Sens. Actuators B **B77**, 579 (2001).
[4] D. C. Meier, C. J. Taylor, R. E. Cavicchi, W. V. Edward, M. W. Ellzy, K. B. Sumpter, and S. Semancik, IEEE Sens. J. **5**, 712 (2005).
[5] Z. Boger, D. C. Meier, R. E. Cavicchi, and S. Semancik, Sens. Lett. **1**, 86 (2003).
[6] O. Sneh and S. M. George, J. Phys. Chem. **99**, 4639 (1995).
[7] R. E. Cavicchi, G. E. Poirier, J. S. Suehle, M. Gaitan, S. Semancik, and D. R. F. Burgess, J. Vac. Sci. Technol. A **12**, 2549 (1994).
[8] P. R. Norton, J. A. Davies, D. K. Creber, C. W. Sitter, and T. E. Jackman, Surf. Sci. **108**, 205 (1981).
[9] B. Kasemo and E. Toernqvist, Phys. Rev. Lett. **44**, 1555 (1980).
[10] P. A. Redhead, Vacuum **12**, 203 (1962).
[11] D. A. King, Surf. Sci. **47**, 384 (1975).

[12]J. T. Yates, in *Methods of Experimental Physics*, Solid State Physics: Surfaces Vol. 22, edited by R. L. Park and M. G. Lagally (Academic, Orlando, 1985), pp. 425–464.
[13]A. M. De Jong and J. W. Niemantsverdriet, Surf. Sci. **233**, 355 (1990).
[14]E. Habenschaden and J. Kueppers, Surf. Sci. **138**, L147 (1984).
[15]J. L. Falconer and R. J. Madix, J. Catal. **48**, 262 (1977).
[16]J. L. Taylor and W. H. Weinberg, Surf. Sci. **78**, 259 (1978).
[17]V. P. Zhdanov, Surf. Sci. Rep. **12**, 183 (1991).
[18]S. Ma, F. G. Amar, and B. G. Frederick, J. Phys. Chem. A **107**, 1413 (2003).
[19]B. Meng and W. H. Weinberg, J. Chem. Phys. **100**, 5280 (1994).
[20]D. L. S. Nieskens, A. P. van Bavel, and J. W. Niemantsverdriet, Surf. Sci. **546**, 159 (2003).
[21]M. A. DeAngelis and A. B. Anton, J. Vac. Sci. Technol. A **10**, 3507 (1992).
[22]R. H. Jackson, Ph.D. thesis, University of Maine, 2000.
[23]P. B. Weisz, J. Chem. Phys. **21**, 1531 (1953).
[24]B. G. Frederick, F. M. Leibsle, S. Haq, and N. V. Richardson, Surf. Rev. Lett. **3**, 1523 (1996).
[25]B. G. Frederick, Q. Chen, F. M. Leibsle, M. B. Lee, K. J. Kitching, and N. V. Richardson, Surf. Sci. **394**, 1 (1997).
[26]J. Lee, O. Kuzmych, and J. T. Yates, Surf. Sci. **582**, 117 (2005).
[27]M. Y. Afridi, J. S. Suehle, M. E. Zaghloul, D. W. Berning, A. R. Hefner, R. E. Cavicchi, S. Semancik, C. B. Montgomery, and C. J. Taylor, IEEE Sens. J. **2**, 644 (2002).
[28]Q. Guo, I. Cocks, and E. M. Williams, Surf. Sci. **393**, 1 (1997).
[29]E. G. Seebauer, and C. E. Allen, Prog. Surf. Sci. **49**, 265 (1995).
[30]Z. Wang and E. G. Seebauer, Appl. Surf. Sci. **181**, 111 (2001).
[31]Y. Lilach, I. M. Danziger, and M. Asscher, Catal. Lett. **76**, 35 (2001).
[32]M. W. de Lange, J. G. van Ommen, and L. Lefferts, Appl. Catal., A **220**, 41 (2001).
[33]D. R. Lide, *CRC Handbook of Chemistry and Physics*, 87th ed. (Taylor and Francis Group, London/CRC, Boca Raton, FL, 2006), section 5, p. 34.